RSC Advances

PAPER

View Article Online
View Journal | View Issue

Cite this: *RSC Adv.*, 2019, **9**, 26043

Two AIEE-active α-cyanostilbene derivatives containing BF_2 unit for detecting explosive picric acid in aqueous medium†

Shengmei Guo,[a] Jianting Pan,[ab] Jianyan Huang,[a] Lin Kong [a] and Jiaxiang Yang *[a]

Received 5th July 2019
Accepted 12th August 2019

DOI: 10.1039/c9ra05116c

rsc.li/rsc-advances

Two novel α-cyanostilbene derivatives bearing triphenylamine and BF_2 groups are synthesized (named **TPE-B** and **TPE-BN**). The fluorescent emissions of compounds **TPE-B** and **TPE-BN** are hypochromatically shifted and bathochromically shifted, respectively, with increasing polarity of the solvents, suggesting that the two compounds have characteristic polarity-dependent solvatochromic effects. Furthermore, they show obvious aggregation-induced emission enhancement (AIEE) phenomenon in THF/water mixture solutions. Meanwhile, compounds **TPE-B** and **TPE-BN** emit orange and yellow fluorescence in their solid states, respectively. Most significantly, in aqueous medium, compounds **TPE-B** and **TPE-BN** can selectively and sensitively detect picric acid (PA) among a number of nitroaromatic compounds, and their limits of detection (LOD) are calculated as 1.26×10^{-6} M and 1.51×10^{-6} M, respectively. The recognition mechanism for PA can be attributed to the photo-induced electron transfer (PET) process and this is supported by density functional theory (DFT) calculation. This research provides two novel compounds for the rational design of AIEE-active materials for sensing systems.

1. Introduction

During the past decade, aesthetic organic fluorophores with aggregation induced emission (AIE) or aggregation-induced enhanced emission (AIEE) properties have received intense attention by virtue of their extensive applications as imaging agents and sensors, components of light-emitting diodes, and data recording and storage, among others.[1–8] Developing functional AIE/AIEE materials can provide several advantages over conventional materials, such as their high quantum yields, controlled self-assembly effects, photostabilities, controllable emission colour, and flexible post-functionalization such as tetraphenylethene, α-cyanostilbene, silole, diphenyldibenzofulvene, organoboron, phosphindole oxide, pyrazine, phenothiazine derivatives, *etc*[9–13]. The twisted molecular conformations of organic fluorophores can emit strong fluorescence in the aggregated state by suppressing a dense face-to-face packing and immense π–π stacking interaction. Also, in the aggregated state, the molecules interlock themselves which restricts the intramolecular rotation (RIR) and vibration (RIV) and relaxes through radiative pathways.[14–21] Therefore, it is of great significance to design and understand the relationships between structure and property for their further applications.[22–24]

For the purpose of obtaining eminent organic molecules with strong fluorescence in aggregated states, the molecular design according to organic fluorophores is critical for adjusting their photophysical properties. Triphenylamine (TPA) is strong electron-donating structural units with good luminescence properties, high thermal, photostability, good absorptivity, and high absolutely quantum yields.[25–27] Furthermore, an organoboron compound allowing trigonal-planar geometry, endows high extinction coefficients and high absolutely fluorescence quantum yields.[28–31,55] The combination of α-cyanostilbene modified with triphenylamine and BF_2 groups were used to design AIEE-active compounds **TPE-B** and **TPE-BN** (Scheme 1).[32–34] In the present investigation, it was found that picric acid (PA) is a powerful explosive as TNT, only a few available PA

[a]*College of Chemistry & Chemical Engineering, Anhui University, Anhui Province Key Laboratory of Chemistry for Inorganic/Organic Hybrid Functional Materials, Hefei 230601, P. R. China. E-mail: jxyang@ahu.edu.cn*

[b]*Anhui Province Institute of Product Quality Supervision & Inspection, Hefei 230051, P. R. China*

† Electronic supplementary information (ESI) available: Photophysical properties; the Sterne–Volmer plots; UV-vis spectra in THF/H_2O mixtures. PL emission spectra changes of **TPA-B** in THF/H_2O mixtures; photophysical properties of PA detection for compound **TPA-BN**; normalized absorption spectrum of PA and the fluorescence spectra of **TPE-B** and **TPE-BN**. See DOI: 10.1039/c9ra05116c

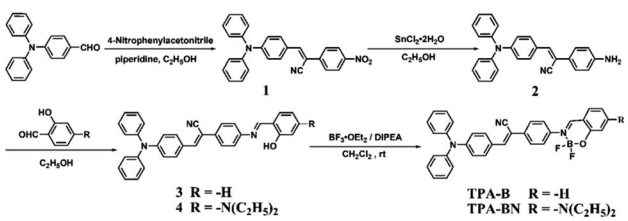

Scheme 1 Synthetic routes of compounds TPE-B and TPE-BN.

sensing reports in aqueous medium. Meanwhile, PA is a seriously environmental pollutant, which consequently causes damage of human health and aquatic systems.[35–39] We expect two compounds to exhibit brilliant PA detection in aqueous medium.

Based on the above considerations, two α-cyanostilbene derivatives (named **TPE-B** and **TPE-BN**) were synthesized *via* facile reaction. The UV-vis absorption spectra and fluorescence spectra of compounds **TPE-B** and **TPE-BN** were systematically investigated in different polar solvents. Meanwhile, the aggregates emission behaviors of compounds were studied in THF/water mixture solution. In addition, the recognition properties of **TPA-B** and **TPA-BN** to PA were studied and the corresponding sensor mechanism was analyzed by density functional theory (DFT) calculations.

2. Experimental section

2.1 Materials and instruments

The chemicals and solvents were purchased from a commercial supplier and used directly without any further refinement. The ^{1}H and ^{13}C NMR spectra were identified by a Bruker Avance 400 MHz spectrometer with tetramethylsilane as the internal standard. FT-IR spectra were obtained by Nicolet 380 spectrometer (4000–400 cm^{-1}, KBr pellets). UV-vis absorption spectra were measured using a TU-1901 spectrometer and the fluorescence spectra were collected by Hitachi FL-7000 spectrofluorimeter from Hitachi High Technologies Corporation (Tokyo, Japan). Photo images were obtained using a digital camera (Nikon D7000).

2.2 Synthesis

The synthetic routes of compounds **TPE-B** and **TPE-BN** are shown in Scheme 1.

2.2.1. Synthesis of compound 1. The 4-*N*,*N*-diphenylaminobenzaldehyde (410 mg, 1.50 mmol) and *p*-nitrophenylacetonitrile (240 mg, 1.50 mmol) were dissolved in absolute ethanol (40 mL). After adding 2 drops of piperidine, the reaction mixture was refluxed for 5 h. After cooling to room temperature, the red precipitate was filtered, washed with ethanol for three times. The final product was dried in vacuum and collected as red powder **1** (290 mg, 0.69 mmol, yield: 46%). ^{1}H NMR (DMSO-d_6, 400 MHz) δ (ppm): 6.95 (d, J = 7.9 Hz, 2H), 7.17–7.23 (m, 6H), 7.42 (t, J = 7.9 Hz, 4H), 7.92 (d, J = 8.4 Hz, 2H), 7.98 (d, J = 8.0 Hz, 2H), 8.15 (s, 1H), 8.32 (d, J = 8.4 Hz, 2H). ^{13}C NMR (DMSO-d_6, 100 MHz) δ (ppm): 103.70, 118.01, 119.21, 124.29, 125.10, 125.22, 125.96, 126.30, 129.94, 131.52, 140.84, 145.56, 145.69, 146.75, 150.37.

2.2.2 Synthesis of compound 2. Compound **1** (250 mg, 0.60 mmol) and $SnCl_2 \cdot 2H_2O$ (680 mg, 3.01 mmol) were reflux under absolute ethanol (40 mL) for 2 hours. After cooling to room temperature, the mixture was poured into a saturated K_2CO_3 aqueous solution and extracted with dichloromethane. The organic layer was dried with $MgSO_4$ and concentrated by vacuum evaporation. The crude product was purified by column chromatography (petroleum ether : ethyl acetate = 2 : 1). The final product was dried in vacuum and collected as orange powder **2** (180 mg, 0.46 mmol, yield: 76%). ^{1}H NMR (DMSO-d_6, 400 MHz) δ (ppm): 5.57 (s, 2H), 6.55 (d, J = 8.0 Hz, 1H), 6.63 (d, J = 8.4 Hz, 1H), 6.73 (d, J = 7.9 Hz, 1H), 6.96 (d, J = 8.3 Hz, 2H), 7.03–7.08 (m, 2H), 7.10–7.19 (m, 5H), 7.35–7.40 (m, 4H), 7.57 (s, 1H), 7.76 (d, J = 8.4 Hz, 2H). ^{13}C NMR (DMSO-d_6, 100 MHz) δ (ppm): 107.71, 113.90, 118.78, 120.84, 121.25, 124.15, 125.09, 126.45, 127.40, 129.73, 129.95, 136.21, 146.31, 148.35, 149.67. MALDI-TOF calcd for $C_{27}H_{21}N_3$, 387.170, found, 387.947.

2.2.3 Synthesis of compounds 3 and 4. A 50 mL round bottom flask was charged with compound **2** (580 mg, 1.50 mmol), aldehyde (1.80 mmol) and absolute ethanol (70 mL). A dropwise glacial acetic acid was added into the mixture solution. The mixture solution was refluxed for 12 h. After cooling to room temperature, the precipitate was filtered. The final product was dried in vacuum and collected.

Red powder **3** (530 mg, 1.08 mmol, yield: 72%). FT-IR (cm^{-1}, KBr) ν: 3423, 2211, 1618, 1581, 1535, 1332, 1285, 1196, 1178, 902, 829, 753, 696, 621, 535, 511. ^{1}H NMR ($CDCl_3$, 400 MHz) δ (ppm): 6.94–6.98 (m, 2H), 7.04 (d, J = 9.2 Hz, 2H), 7.19–7.23 (m, 7H), 7.38–7.47 (m, 5H), 7.62 (d, J = 7.6 Hz, 1H), 7.79–7.87 (m, 4H), 7.92 (d, J = 9.2 Hz, 2H), 8.99 (s, 1H), 13.06 (s, 1H). ^{13}C NMR ($CDCl_3$, 100 MHz) δ (ppm): 106.78, 117.31, 118.63, 119.19, 120.74, 121.80, 124.45, 125.44, 125.74, 126.25, 126.67, 129.57, 130.71, 132.44, 133.43, 133.62, 141.38, 146.52, 148.41, 150.03, 161.22, 162.78. MALDI-TOF calcd for $C_{34}H_{25}N_3O$, 491.200, found, 491.671.

Red powder **4** (590 mg, 1.04 mmol, yield: 69%). FT-IR (cm^{-1}, KBr) ν: 3430, 2965, 2924, 2210, 1633, 1558, 1520, 1375, 1193, 1177.69, 1133, 1076, 874, 972, 845, 751, 727. ^{1}H NMR ($CDCl_3$, 400 MHz) δ (ppm): 1.18–1.22 (m, 6H), 3.45–3.50 (m, 4H), 6.15 (s, 1H), 6.37 (d, J = 8.7 Hz, 2H), 7.03 (d, J = 8.8 Hz, 2H), 7.16–7.20 (m, 6H), 7.31 (d, J = 8.8 Hz, 2H), 7.37–7.43 (m, 5H), 7.77 (d, J = 8.6 Hz, 3H), 7.91 (d, J = 8.3 Hz, 2H), 8.70 (s, 1H), 13.40 (s, 1H). ^{13}C NMR ($CDCl_3$, 100 MHz) δ (ppm): 12.73, 44.65, 97.78, 104.05, 107.36, 109.16, 118.74, 120.98, 121.35, 124.34, 125.68, 126.15, 126.62, 129.56, 130.59, 132.69, 133.78, 133.99, 140.62, 146.67, 149.85, 152.12, 160.49, 164.21. MALDI-TOF calcd for $C_{38}H_{34}N_3O$, 562.273, found, 562.995.

2.2.4 Synthesis of compounds TPA-B and TPA-BN. The compound **3** or **4** (1.0 mmol) and *N*,*N*-diisopropylethylamine (DIPEA, 1 mL) were dissolved in CH_2Cl_2 (10 mL) and the reaction was stirred at room temperature for 2 h. Then, $BF_3 \cdot OEt_2$ (1.5 mL) was dropwise added into the mixture solution. The reaction mixture was stirred and monitored by TLC until completed. The mixture was poured into cold water (80 mL), extracted with CH_2Cl_2 and dried with $MgSO_4$. After the solvent is evaporated under reduced pressure. The solid was obtained by chromatography on a silica gel column using DCM as the eluent.

Orange red powder **TPA-B** (400 mg, 0.75 mmol, yield: 75%). FT-IR (cm^{-1}, KBr) ν: 3056, 2923, 2853, 2217, 1627, 1583, 1556, 1534, 1459, 1389, 1331, 1329, 1270, 1216, 1179, 1153, 1047, 758, 698, 530, 512. ^{1}H NMR ($CDCl_3$, 400 MHz) δ (ppm): 5.53 (s, 3H), 6.83 (d, J = 7.5 Hz, 1H), 7.03–7.18 (m, 8H), 7.29–7.35 (m, 3H), 7.48 (s, 1H), 7.53 (t, J = 7.4 Hz, 1H), 7.59 (s, 1H), 7.63 (d, J = 7.9 Hz, 1H), 7.69 (t, J = 8.0 Hz, 1H), 7.76–7.81 (m, 3H), 8.48 (s,

1H). ^{13}C NMR ($CDCl_3$, 100 MHz) δ (ppm): 105.76, 118.35, 120.53, 120.61, 124.12, 124.42, 124.66, 125.54, 125.76, 125.90, 126.83, 129.47, 129.54, 129.63, 130.22, 131.02, 132.26, 136.09, 139.58, 143.02, 146.42, 150.50. MALDI-TOF calcd for $C_{34}H_{24}BF_2N_3O$, 538.202, found, 538.595.

Yellow powder **TPA-BN** (410 mg, 0.66 mmol, yield: 66%). FT-IR (cm^{-1}, KBr) ν: 3035, 2975, 2929, 2204, 1626, 1589, 1509, 1459, 1352, 1313, 1297, 1278, 1241, 1217, 1192, 1145, 1075, 1030, 971, 961, 898, 842, 750, 729, 529. ^{1}H NMR ($CDCl_3$, 400 MHz) δ (ppm): 1.23–1.27 (m, 6H), 3.49–3.44 (m, 4H), 6.25 (s, 1H), 6.38 (d, J = 9.2 Hz, 1H), 6.82 (d, J = 8.6 Hz, 1H), 7.04–7.17 (m, 9H), 7.28–7.34 (m, 4H), 7.43 (s, 1H), 7.51 (s, 1H), 7.56 (d, J = 8.4 Hz, 1H), 7.23 (s, 1H), 7.69 (d, J = 8.5 Hz, 1H), 7.79 (d, J = 8.6 Hz, 1H), 8.06 (s, 1H). ^{13}C NMR ($CDCl_3$, 100 MHz) δ (ppm): 12.69, 45.24, 98.03, 106.40, 106.97, 107.17, 118.58, 120.75, 123.49, 124,51, 125.79, 126.22, 126.57, 129.62, 130.86, 134.17, 134.20, 142.03, 143.11, 146.55, 150.16, 156.48, 157.52, 161.96. MALDI-TOF calcd for $C_{38}H_{33}BF_2N_4O$, 609.271, found, 609.830.

3. Results and discussion

3.1 Solvatochromic effect

The UV-vis absorption and photoluminescence (PL) spectra of compounds **TPA-B** and **TPA-BN** were measured in various polar solvents and demonstrated in Fig. S1† and Fig. 1, respectively, and the corresponding photophysical data were summarized in Table 1. All the spectroscopic studies were performed at room temperature and the concentration of the solutions were 1.0×10^{-5} mol L^{-1}. The UV-vis absorption spectra of **TPA-BN** showed two characteristic absorption bands at 297 nm and 420 nm in various polarity solvents, respectively. The absorption peak at 297 nm is ascribed to the π–π* transition in TPA moiety corresponding to locally excited (LE) state,[27,40,41] while the latter peak at 420 nm denotes intramolecular charge transfer (ICT) process. The UV-vis absorption of **TPA-B** has a similar peak shapes. And the emission wavelengths of two compounds revealed larger shift with increasing polarity. For compound **TPA-B**, the emission peak was hypochromatic-shifted from 541 nm in benzene to 530 nm in ethanol, indicated that **TPA-B** molecule possibly had a larger polarity in the ground state than in the excited state. However, the fluorescent emission peak of compound **TPA-BN** was bathochromic-shifted from 516 nm in benzene to 540 nm in DMF, indicated that **TPA-BN** molecule might have a larger polarity in the excited state than in the ground state.[42–44] Meanwhile, the evident shift of emission peaks manifested the existence of ICT process. The slopes of the fitting line in Lippert–Mataga plots (Fig. S2†), which were −646.5 and 2887.8, respectively, indicated that the compound **TPA-BN** introduced into the electron-donating group significantly possessed the solvatochromic effects. And, Fig. 5 shows that the TPA group has a larger density in the highest occupied frontier molecular orbital (HOMO) of **TPA-B** molecular. As the electron density of the lowest unoccupied molecular orbital (LUMO) of the TPA unit decreases, the other moieties achieve larger electron density. For **TPA-BN**, the HOMO and LUMO were mostly distributed over the molecular and TPA groups, respectively, which further manifested that the ICT process might occur in **TPA-B** and **TPA-BN**.[60] It was indicated that two compounds were characteristic of polarity-dependent solvatochromic effects.

Table 1 Photophysical properties of compounds TPA-B and TPA-BN in different polar solvents

Compounds	Solvents	λ_{abs} [a]	ε_{max} [b]	λ_{fl} [c]	$\Delta\nu$ [d]	Φ [e] (%)
TPA-B	Benzene	419	4.59	541	5382	8.8
	DCM	427	7.10	538	4832	1.0
	Ethyl acetate	420	6.64	570	6262	2.3
	THF	420	6.76	531	4977	1.5
	Ethanol	408	6.06	530	5642	1.2
	Acetonitrile	420	7.19	535	5118	0.1
	DMF	423	7.07	540	5122	0.1
TPA-BN	Benzene	423	7.78	516	4260	9.1
	DCM	418	7.93	533	5161	6.1
	Ethyl acetate	415	7.81	519	4828	8.8
	THF	416	7.75	520	4807	4.2
	Ethanol	414	7.59	526	5143	6.9
	Acetonitrile	422	8.76	542	5246	1.2
	DMF	425	7.66	540	5010	3.1

[a] Absorption peak position in nm (1×10^{-5} mol L^{-1}). [b] Maximum molar absorbance in 10^4 mol^{-1} L cm^{-1}. [c] Peak position of fluorescent (1.0×10^{-5} mol L^{-1}), excited at the absorption maximum. [d] Stokes shift in cm^{-1}. [e] Quantum yields determined (RhB as the standard).

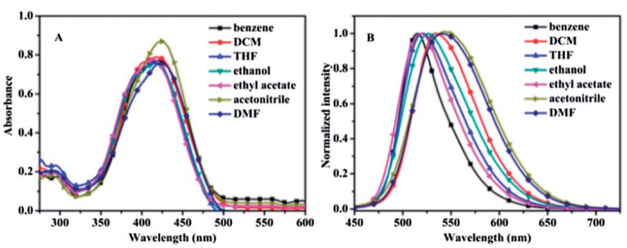

Fig. 1 UV-vis absorption spectra (A) and PL spectra (B) of the compound TPA-BN in different solvent.

3.2 Aggregation-induced emission enhancement (AIEE) property

Aiming to investigate the AIEE characteristics of **TPA-B** and **TPA-BN**, their UV-vis absorption spectra and PL spectra with different water fraction were performed. The concentrations were kept at 1.0×10^{-5} mol L^{-1}. For UV-vis absorption spectra of compound **TPA-BN** (Fig. S3b†), with the increasing water fraction, the solubility of the compound gradually decreased and the molecules gradually shifted from the monomolecular state to the aggregation state, forming the molecular aggregated particles. The level-off tails attributed to Mie scattering were responsible for the aggregated forms in the UV-vis absorption spectra.[45–50] A similar change trend was also observed from the UV-vis absorption spectra of **TPA-B** with the change of water contents. For compounds **TPA-B** and **TPA-BN**, dynamic light scattering (DLS) experiment displays the formation of aggregates (the hydrodynamic diameter of 267.2 nm and 390.2 nm, respectively). For PL spectra (Fig. 2), in pure THF solution,

compound **TPA-BN** emitted weak yellow-green fluorescence. Compound **TPA-BN** started gradually aggregate with the increasing water fraction, the PL intensity showed a remarkable enhancement accompanied with a bathochromic-shift of fluorescent emission peak. This emission behavior may be accounted for the restriction of intramolecular rotation (RIR) and forms of *J*-aggregation,[51] which blocks the channel of non-radiative decay in the aggregates. Furthermore, when the water fraction is higher than 80%, the PL intensities gradually decreased, because the settlement of large aggregated particles resulted in a lower fluorescence intensity. Moreover, we found that the PL spectra of the compound **TPA-B** (Fig. S4†) displayed a similar behavior. The PL intensity of the compounds **TPA-B** and **TPA-BN** in the aggregated state were obviously stronger than that of the THF solution, the PL intensities were 1.6 and 2.0 fold, respectively. It was easily concluded that compounds **TPA-B** and **TPA-BN** were typical AIEE-active molecules.

Furthermore, PL spectra of compounds **TPA-B** and **TPA-BN** were investigated to explore the difference of solid emission. As was shown in Fig. 3, **TPA-B** exhibited orange emission, whereas **TPA-BN** containing an additional electron-donating group has a obvious influence on hypsochromic shift of fluorescent peaks, emitting yellow fluorescence. The solid state fluorescent quantum yields of **TPA-B** and **TPA-BN** were measured as 13.5% and 19.4%, respectively in the solid state. The possible fluorescence emission discrepancy was caused by the role of intermolecular arrangement and stacking in solid state. Thus, the introduction of additional electron-donating group could effectively affect their fluorescence emission behavior and result in different spectral shifts and absolute quantum yields.

3.3 The detection for picric acid

Based on brilliant AIEE behavior of compounds **TPA-B** and **TPA-BN** in mixtures of THF/H_2O. We next explore whether compounds **TPA-B** and **TPA-BN** can detect common nitroaromatic compounds (*p*-methyl phenol (*p*-MP), *o*-nitrophenol (*o*-NP), 2,4,6-trinitrotoluene (TNT), *m*-dihydroxybenzene (*m*-DOB), *p*-nitrophenol (*p*-NP), *p*-dihydroxybenzene (*p*-DOB), phenol (PhOH), *p*-nitroaniline (*p*-NA), nitrotoluene (NT), nitrobenzene (NB), 2,4,6-trinitrophenol (PA)) in aqueous medium, the PL spectra were measured with addition of 10 equivalents nitroaromatic compounds. As shown in Fig. 4a and S6a,† compared with other analytes, it was clearly observed that the positive interactions of **TPA-B** and **TPA-BN** with PA showed significant fluorescent quenching effect. Experimental results exhibited that other nitroaromatics exhibited relatively little effect on emission quenching compared with that of PA, suggesting the selective sensing behaviors of **TPA-B** and **TPA-BN** towards PA. Furthermore, it is worth noting that further additions of 10 equivalents PA into other nitroaromatic systems leads to remarkable quenching efficiency of fluorescence intensity (Fig. 4b and S6b†), means that other compounds have negligible effect on the detection of PA by **TPA-B** and **TPA-BN**. According to the above results, compounds **TPA-B** and **TPA-BN**

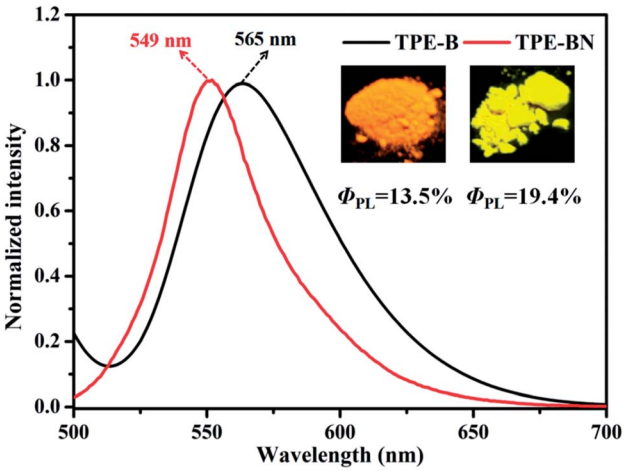

Fig. 3 Normalized PL spectra of two solids. Inset: the corresponding fluorescence images of TPA-B and TPA-BN under illumination.

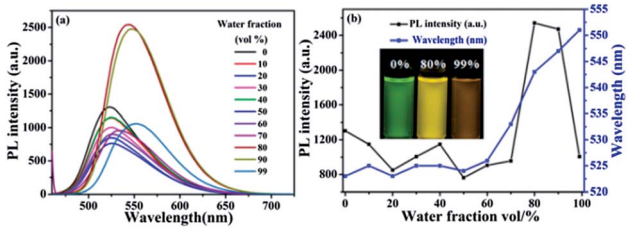

Fig. 2 PL emission (a) spectra changes of **TPA-BN** (5.0×10^{-5} M) in THF/H_2O mixtures with different water volume fractions; plots of PL intensity determined in THF–H_2O solutions *versus* water fractions (b). Insets: photos of **TPA-BN** in THF–H_2O mixtures (f_w = 0%, 80% and 99%) taken under 365 nm UV lamp.

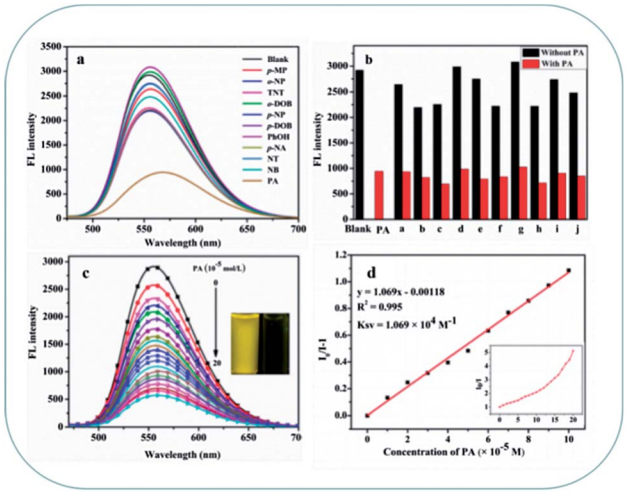

Fig. 4 (a) PL spectra obtained for different analytes; (b) quenching percentages of compound **TPA-BN** (10.0 μM) with different analytes in THF/water (v/v = 2 : 8) mixtures before (black) and after (red) the addition of 10 equiv. a: *p*-MP, b: *o*-NP, c: TNT, d: *m*-DOB, e: *p*-NP, f: *p*-DOB, g: PhOH, h: *p*-NA, i: NT, j: NB; (c) PL spectra of TPA-BN (10.0 μM) in THF/water (v/v = 2 : 8) containing different amounts of PA (100.0 μM); (d) corresponding Stern–Volmer plot for PA detection. Inset: Stern–Volmer plot obtained at a lower concentration of PA.

are regarded as promising candidates for PA detection in aqueous medium.

The key to performing better practical application, the experiment was carried out to better explore the sensitivity of compounds **TPA-B** and **TPA-BN** towards PA in aqueous medium. As shown in Fig. 4c and Fig. S6c,† the fluorescent quenching efficiencies of **TPA-B** and **TPA-BN** were 82.7% and 81.6% in the presence of 10 equivalents PA, respectively. In order to evaluate the quenching efficiency of **TPA-B** and **TPA-BN** in response to the PA in solution, a quenching process can be analyzed by Stern–Volmer equation,[52] the equation was as follow:

$$I_0/I = K_{sv}[A] + 1$$

where I_0 and I are the initial and final PL intensity after addition of PA, respectively; [A] is the molar concentration of analytes; and K_{sv} is the Stern–Volmer quenching constant. By fitting the linear curves, the slopes of the plots gave the K_{sv} of **TPA-BN** and **TPA-B**, which were 1.28×10^4 M^{-1} and 1.07×10^4 M^{-1}, respectively. The limit of detection (LOD)[53,54] was obtained from the equation of LOD = $3\sigma/k$, wherein σ is the standard deviation of the blank test, k represents the slope of the linear calibration curve, the LOD were calculated as 1.26×10^{-6} M for **TPA-B** and 1.51×10^{-6} M for **TPA-BN**, respectively (Fig. S7†). Compounds exhibiting brilliant PA detection in aqueous medium are comparable with organoboron chemosensors in the Table S1.†[56–59]

Density functional theory (DFT) calculation was used to investigate possible PA sensing mechanism. As shown in Fig. 5, the LUMO level (−2.79 eV) of **TPA-B** is higher than that of PA (−3.90 eV), which suggested when excited **TPA-B** was exposed to PA, the excited electron was transferred from the LUMO of fluorophores to that of the electron-deficient PA. The radiative electronic transition was blocked due to the electron transfer from the chromophore to PA, resulting in fluorescence quenching. Moreover, the other driving force is the energy difference between the LUMO of the fluorophore and the LUMO of analytes.[61–65] The LUMO orbital energy typically indicates how easily an electron can be transferred from excited fluorophore to the electron-deficient analytes. As the LUMO orbital energies of PA and TNT calculated by DFT is −3.90 eV and −3.33 eV, respectively. As expected, because of its small LUMO value, the PET driving force of PA is larger than that of TNT. This may partly explain the sensitivity and selectivity of **TPA-B** for PA detection. Similarly, for **TPA-BN**, the LUMO energy level of PA is between the LUMO energy level and the HOMO energy level of **TPA-BN**, indicating that the fluorescence quenching of **TPA-BN** with PA may suggest that the possibility of electron transfer from the LUMO of the chemosensor to the lower LUMO of PA. Based on the above results, the main driving force was attributed to the photo-induced electron transfer (PET) process, resulting in fluorescence quenching. Meanwhile, as was showed in the Fig. S8,† the UV-vis absorption spectra of PA and the PL spectra of **TPA-B** and **TPA-BN** were recorded and presented to examine whether fluorescence resonance energy transfer (FRET) occurs in detection process. The absorption spectrum of PA has no overlap with the PL spectra of the two chemosensors, indicating that FRET was neglectable in the quenching process. Therefore, the PET process may be main reason for recognition mechanism between the chemosensors and PA.

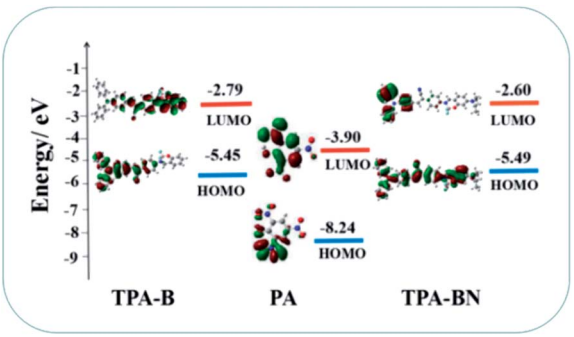

Fig. 5 HOMO and LUMO energy–level diagram of TPA-B/TPA-BN and PA.

4. Conclusions

In conclusion, two novel α-cyanostilbene derivatives (**TPA-B** and **TPA-BN**) containing triphenylamine and BF_2 units are synthesized and characterized that displayed obvious solvatochromic effect. Their ICT behaviors are certified by DFT analysis on molecular orbitals. Meanwhile, the incorporation of α-cyanostilbene unit in the backbone endows molecules an obvious AIEE behaviour in THF–water mixture solvent. Compounds showed excellent fluorescence emission in the solid state with high absolute quantum yield. Most impressing, **TPA-B** and **TPA-BN** were used as highly selectively and sensitively chemosensor to detect PA in aqueous medium and the LODs were calculated as 1.26×10^{-6} M and 1.51×10^{-6} M, respectively. The efficient sensing mechanism of two chemosensors in the presence of PA contributed to the PET process, verified by DFT calculations on molecular orbitals. This research provides two novel compounds for the rational design of AIEE-active materials for sensing application in aqueous medium.

Conflicts of interest

We declare that we do not have any commercial or associative interest that represents a conflict of interest in connection with the work submitted.

Acknowledgements

This work was supported by the National Natural Science Foundation of China (51673001, 51432001), the Educational Commission of Anhui Province of China (KJ2014ZD02).

References

1 V. Mahendran, K. Pasumpon, S. Thimmarayaperumal, P. Thilagar and S. Shanmugam, Tetraphenylethene-2-pyrone conjugate: aggregation-induced emission study and explosives sensor, *J. Org. Chem.*, 2016, **81**, 3597–3602.

2 J. D. Luo, Z. L. Xie, J. W. Y. Lam, L. Cheng, H. Y. Chen, C. F. Qiu, H. S. Kwok, X. W. Zhan, Y. Q. Liu, D. B. Zhu and B. Z. Tang, Aggregation-induced emission of 1-methyl-1,2,3,4,5-pentaphenylsilole, *Chem. Commun.*, 2001, 1740–1741.

3 K. Li, Y. Zhang, B. Qiao, F. R. Tao, T. D. Li, Y. Q. Ding, F. M. Raymo and Y. Z. Cui, Facile fabrication of AIE/AIEE-active fluorescent nanoparticles based on barbituric for cell imaging Applications, *RSC Adv.*, 2017, **7**, 30229–30241.

4 H. W. Ma, C. Y. He, X. L. Li, O. Ablikim, S. T. Zhang and M. Zhang, A fluorescent probe for TNP detection in aqueous solution based on joint properties of intramolecular charge transfer and aggregation-induced enhanced emission, *Sens. Actuators, B*, 2016, **230**, 746–752.

5 Z. J. Ning, Z. Chen, Q. Zhang, Y. L. Yan, S. X. Qian, *et al.*, Aggregation-induced emission(AIE)-active starburst triarylamine fluorophores as potential non-doped red emitters for organic light-emitting diodes and Cl_2 gas chemodosimeter, *Adv. Funct. Mater.*, 2007, **17**, 3799–3807.

6 B. H. Yu, D. Y. Liu, Y. Wang, T. Zhang, Y. M. Zhang and M. J. Lia, A solid-state emissive and solvatofluorochromic fluorophore and its application in high-contrast, fast, and repeatable thermochromic blends, *Dyes Pigm.*, 2019, **163**, 412–419.

7 S. Gupta and M. D. Milton, Design and synthesis of novel V-shaped AIEE active quinoxalines for acidochromic applications, *Dyes Pigm.*, 2019, **165**, 474–487.

8 B. K. An, S. K. Kwon, S. D. Jung and S. Y. Park, Enhanced emission and its switching in fluorescent organic nanoparticles, *J. Am. Chem. Soc.*, 2002, **124**, 14410–14415.

9 S. Kandel, V. Sathish, L. Mathivathanan, A. N. Morozov, A. M. Mebel and R. G. Raptis, Aggregation induced emission enhancement (AIEE) of tripodal pyrazole derivatives for sensing of nitroaromatics and vapor phase detection of picric acid, *New J. Chem.*, 2019, **43**, 7251–7258.

10 C. X. Niu, Y. You, L. Zhao, D. C. He, N. Na and O. Y. Jin, Solvatochromism, reversible chromism and self-assembly effects of heteroatom-assisted aggregation-induced enhanced emission (AIEE) compounds, *Chem. –Eur. J.*, 2015, **21**, 13983–13990.

11 X. F. Mei, G. X. Wen, J. W. Wang, H. M. Yao, Y. Zhao, Z. H. Lin and Q. D. Ling, A K-shaped donor-π-acceptor-π-donor molecule with AIEE and CIEE activity and sequential logic gate behaviour, *J. Mater. Chem. C*, 2015, **3**, 7267–7271.

12 J. Mei, N. L. C. Leung, R. T. K. Kwok, J. W. Y. Lam and B. Z. Tang, Aggregation-induced emission: together we shine, united we soar!, *Chem. Rev.*, 2015, **115**, 11718–11940.

13 T. B. Rajua, P. Gopikrishn, J. V. Vaghasiyac, S. S. Sonic and P. K. Iyer, The solvatochromism and aggregation-induce enhanced emission of triphenylamine substituted styrene derivatives and its application in dye sensitized solar cells, *J. Photochem. Photobiol., A*, 2019, **376**, 12–21.

14 Y. Okazawa, K. Kondo, M. Akita and M. Yoshizawa, Polyaromatic nanocapsules displaying aggregation-induced enhanced emissions in water, *J. Am. Chem. Soc.*, 2015, **137**, 98–101.

15 F. Hu, S. D. Xu and B. Liu, Photosensitizers with aggregation-induced emission: materials and biomedical applications, *Adv. Mater.*, 2018, **30**, 1801350–1801379.

16 X. Z. Yan, M. Wang, T. R. Cook, M. M. Zhang, M. L. Saha, Z. X. Zhou, X. P. Li, F. H. Huang and P. J. Stang, Light-emitting superstructures with anion effect: coordination driven self-assembly of pure tetraphenylethylene metallacycles and metallacages, *J. Am. Chem. Soc.*, 2016, **138**, 4580–4588.

17 Z. J. Zhao, J. W. Y. Lamb and B. Z. Tang, Tetraphenylethene: a versatile AIE building block for the construction of efficient luminescent materials for organic light-emitting diodes, *J. Mater. Chem.*, 2012, **22**, 23726–23740.

18 M. Shyamal, P. Mazumdar, S. Maity, S. Samanta, G. P. Sahoo and A. Misra, Highly selective turn-on fluorogenic chemosensor for robust quantification of Zn(II) based on aggregation induced emission enhancement feature, *ACS Sens.*, 2016, **1**, 739–747.

19 J. Chen, C. C. W. Law, J. W. Y. Lam, Y. Dong, S. M. F. Lo, I. D. Williams, D. Zhu and B. Z. Tang, Synthesis, light emission, nanoaggregation, and restricted intramolecular rotation of 1,1-substituted 2,3,4,5-tetraphenylsiloles, *Chem. Mater.*, 2003, **15**, 1535–1546.

20 P. Gopikrishna, N. Meher and P. K. Iyer, Functional 1,8-naphthalimide AIE/AIEEgens: recent advances and prospects, *ACS Appl. Mater. Interfaces*, 2018, **10**, 12081–12111.

21 C. Y. K. Chan, Z. J. Zhao, J. W. Y. Lam, J. Z. Liu, S. Chen, *et al.*, Efficient light emitters in the solid state: synthesis, aggregation-Induced emission, electroluminescence, and sensory properties of luminogens with benzene cores and multiple triarylvinyl peripherals, *Adv. Funct. Mater.*, 2012, **22**, 378–389.

22 F. Marquardt, C. Stöcker, R. Gartzen, E. Heine, H. Keul and M. Möller, Novel antibacterial polyglycidols: relationship between structure and properties, *Polymers*, 2018, **10**, 96–116.

23 G. L. Xu, Q. Wang, J. C. Fang, Y. F. Xu, J. T. Li, L. Huang and S. G. Sun, Tuning the structure and property of nanostructured cathode materials of lithium ion and lithium sulfur batteries, *J. Mater. Chem. A*, 2014, **2**, 19941–19962.

24 Z. Y. Yang, H. M. Zhang, G. B. Pan and L. J. Wan, Effect of the bridge alkylene chain on adlayer structure and property of functional oligothiophenes studied with scanning tunneling microscopy and spectroscopy, *ACS Nano*, 2008, 24743–24749.

25 M. Chen, H. Nie, B. Song, L. Z. Li, J. Z. Sun, *et al.*, Triphenylamine-functionalized tetraphenylpyrazine: facile preparation and multifaceted functionalities, *J. Mater. Chem. C*, 2016, **4**, 2901–2908.

26 Q. Y. Chen, L. Kong, Y. P. Tian, X. Y. Xu, L. M. Yang, G. B. Zhang, W. B. Jia and J. X. Yang, The self-aggregation of fluorophore-triphenylamine nanostructures with tunable luminescent properties: the effect of acidity and rare earth ions, *RSC Adv.*, 2014, **4**, 18981–18988.

27 M. M. Zhang, W. Yang, T. F. Gong, W. Q. Zhou and R. Y. Xue, Tunable AIEE fluorescence constructed from a triphenylamine luminogen containing quinoline application in a reversible and tunable pH sensor, *Phys. Chem. Chem. Phys.*, 2017, **19**, 21672–21682.

28 F. B. Liu, Z. C. Ding, J. Liu and L. X. Wang, An organoboron compound with a wide absorption spectrum for solar cell applications, *Chem. Commun.*, 2017, **53**, 12213–12216.

29 D. T. Yang, S. K. Mellerup, J.-B. Peng, X. Wang, Q. S. Li and S. Wang, Substituent directed phototransformations of BN-heterocycles: elimination vs isomerization via selective B-C bond cleavage, *J. Am. Chem. Soc.*, 2016, **138**, 11513–11516.

30 V. M. Hertz, M. Bolte, H. W. Lerner and M. Wagner, Boron-containing polycyclic aromatic hydrocarbons: facile synthesis of stable, redox-active luminophores, *Angew. Chem., Int. Ed.*, 2015, **54**, 8800–8804.

31 A. K. Vasu, M. Radhakrishna and S. Kanvah, Self-assembly tuning of α-cyanostilbene fluorogens: aggregates to nanostructures, *J. Phys. Chem. C*, 2017, **121**, 22478–22486.

32 J. Q. Liao, M. Yang, Z. Liu and H. L. Zhang, Fast photoinduced deformation of hydrogenbonded supramolecular polymers containing α-cyanostilbene derivative, *J. Mater. Chem. A*, 2019, **7**, 2002–2008.

33 W. B. Jia, P. Yang, J. J. Li, Z. M. Yin, L. Kong, *et al.*, Synthesis and characterization of a novel cyanostilbene derivative and its initiated polymers: aggregation-induced emission enhancement behaviors and light-emitting diode applications, *Polym. Chem.*, 2014, **5**, 2282–2292.

34 Y. Q. Xu, B. H. Li, W. W. Li, J. Zhao, S. G. Sun and Y. Pang, 'ICT-not-quenching' near infrared ratiometric fluorescent detection of picric acid in aqueous media, *Chem. Commun.*, 2013, **49**, 4764–4766.

35 T. M. Geng, Z. M. Zhua, X. Wang, H. Y. Xia, Y. Wang and D. K. Li, Poly{tris[4-(2-thienyl)phenyl]amine} fluorescent conjugated microporous polymer for selectively sensing picric acid, *Sens. Actuators, B*, 2017, **244**, 334–343.

36 K. Li, R. H. Yu, C. M. Shi, F. R. Tao, *et al.*, Electrospun nanofibrous membrane based on AIE-active compound for detecting picric acid in aqueous solution, *Sens. Actuators, B*, 2018, **262**, 637–645.

37 B. Joarder, A. V. Desai, P. Samanta, S. Mukherjee and S. K. Ghosh, Selective and sensitive aqueous-phase detection of 2,4,6-trinitrophenol (TNP) by an amine-functionalized metal-organic framework, *Chem. –Eur. J.*, 2015, **21**, 965–969.

38 A. Biswas, D. Giri, D. Das, A. De, S. K. Patra and R. Samanta, A mild rhodium catalyzed direct synthesis of quinolones from pyridones: application in the detection of nitroaromatics, *J. Org. Chem.*, 2017, **20**(82), 10989–10996.

39 S. Shanmugaraju, D. Umadevi, A. J. Savyasachi, K. Byrne, M. Ruether, W. Schmitt, G. W. Watson and T. Gunnlaugsson, Reversible adsorption and storage of secondary explosives from water using a Troger's base-functionalised polymer, *J. Mater. Chem. A*, 2017, **5**, 25014–25024.

40 J. W. Sun, J. Y. Baek, K. H. Kim, C. K. Moon, J. H. Lee, *et al.*, Thermally activated delayed fluorescence from azasiline based intramolecular charge-transfer emitter (DTPDDA) and a highly efficient blue light emitting diode, *Chem. Mater.*, 2015, **27**, 6675–6681.

41 J. Ohshita, K. Yamamoto, D. Tanaka, M. Nakashima, Y. Kunugi, M. Ohashi and H. Nakano, Preparation and photocurrent generation of silicon nanosheets with aromatic substituents on the surface, *J. Phys. Chem. C*, 2016, **120**, 10991–10996.

42 C. V. Maridevarmath, L. Naik, V. S. Negalurmath, M. Basanagouda and G. H. Malimath, Synthesis, characterization and photophysical studies on novel benzofuran-3-acetic acid hydrazide derivatives by solvatochromic and computational methods, *J. Mol. Struct.*, 2019, **1188**, 142–152.

43 L. Liu, Y. Y. Zhang, J. Zhou, J. H. Yang, C. Zhong, *et al.*, Design of a quinazolinone-based environment-sensitive fluorescent dye: solvatochromic fluorescence and application for one-photon and two-photon bioimaging, *Dyes Pigm.*, 2019, **165**, 58–64.

44 P. Wen, Z. X. Gao, R. Zhang, A. R. Li, F. Zhang, *et al.*, A-π-D-π-A carbazole derivatives with remarkable solvatochromism and mechanoresponsive luminescence turn-on, *J. Mater. Chem. C*, 2017, **5**, 6136–6143.

45 X. D. Liu, A. Li, W. Q. Xu, Z. Y. Ma and X. R. Jia, An ESIPT-based fluorescent switch with AIEE, solvatochromism, mechanochromism and photochromism, *Mater. Chem. Front.*, 2019, **3**, 620–625.

46 P. Zhang, D. D. Li, Y. Li and J. H. Yu, Solvatochromic AIE luminogens as supersensitive water detectors in organic solvents and highly efficient cyanide chemosensors in water, *Chem. Sci.*, 2014, **5**, 2710–2716.

47 M. K. Danquah, S. Wang, Q. Y. Wang, B. Wang and L. D. Wilson, A porous b-cyclodextrin-based terpolymer fluorescence sensor for in situ trinitrophenol detection, *RSC Adv.*, 2019, **9**, 8073–8080.

48 D. Y. Li, X. Y. Zhao, W. Qin, H. Q. Zhang, Y. Fei, L. W. Liu, *et al.*, Toxicity assessment and long-term three-photon fluorescence imaging of bright aggregation-induced emission nanodots in zebrafish, *Nano Res.*, 2016, **7**, 1921–1933.

49 W. Z. Yuan, Y. Y. Gong, S. M. Chen, X. Y. Shen, W. Y. Lam, P. Lu, *et al.*, Efficient solid emitters with aggregation-induced emission and intramolecular charge transfer characteristics: molecular design, synthesis, photophysical behaviors, and OLED application, *Chem. Mater.*, 2012, **24**, 1518–1528.

50 P. Y. Gu, C. J. Lu, Z. J. Hu, N. J. Li, T. T. Zhao, Q. F. Xu, *et al.*, The AIEE effect and two-photon absorption (TPA) enhancement induced by polymerization: synthesis of a monomer with ICT and AIE effects and its homopolymer by ATRP and a study of their photophysical properties, *J. Mater. Chem. C*, 2013, **1**(14), 2599–2606.

51 T. E. Kaiser, V. Stepanenko and F. Wurthner, Fluorescent J-aggregates of core-substituted perylene bisimides: studies on structure-property relationship, nucleation-elongation mechanism, and sergeants-and-soldiers principle, *J. Am. Chem. Soc.*, 2009, **131**, 6719–6732.

52 S. Shanmugaraju, C. Dabadie, K. Byrne, A. J. Savyasachi, *et al.*, A supramolecular Troger's base derived coordination zinc polymer for fluorescent sensing of phenolic-nitroaromatics explosives in water, *Chem. Sci.*, 2017, **8**, 1535–1546.

53 J. Schoo, D. S. Lakshmi, E. Suresh and P. S. Subremanian, Selective and sensitive detection of picric acid in aqueous, sol-gel and solid support media by Ln(III) probes, *Sens. Actuators, B*, 2017, **250**, 215–223.

54 M. Ahmed, S. Hameed, A. Ihsan and M. M. Naseer, Fluorescent thiazol-substituted pyrazoline nanoparticles for sensitive and highly selective sensing of explosive 2,4,6-trinitrophenol in aqueous medium, *Sens. Actuators, B*, 2017, **248**, 57–62.

55 R. Yoshii, K. Tanaka and Y. Chujo, Conjugated polymers based on tautomeric units: regulation of main-chain conjugation and expression of aggregation induced emission property *via* boron-complexation, *Macromolecules*, 2014, **47**, 2268–2278.

56 H. C. Ma, Z. W. Zhang, Y. Y. Jin, L. J. Zha, C. X. Qi, H. Y. Cao, Z. M. Yang, Z. W. Yang and Z. Q. Lei, Triphenylamine-decorated BODIPY fluorescent probe for trace detection of picric acid, *RSC Adv.*, 2015, **5**, 87157–87167.

57 K. Dhanunjayarao, V. Mukundam and K. Venkatasubbaiah, Tetracoordinate imidazole-based boron complexes for the selective detection of picric acid, *Inorg. Chem.*, 2016, **55**, 11153–11159.

58 S. S. Babu and S. Shanmugam, One-pot synthesis of boron diketonate complexes: photophysical properties and sensor for picric acid, *J. Mater. Chem. C*, 2017, **5**, 4788–4796.

59 S. Madhu, A. Bandela and M. Ravikanth, BODIPY based fluorescent chemodosimeter for explosive picric acid in aqueous media and rapid detection in the solid state, *RSC Adv.*, 2014, **4**, 7120–7123.

60 P. C. Xue, B. Q. Yao, J. B. Sun, Z. Q. Zhang, K. C. Li, B. J. Liu and R. Lu, Crystallization-induced emission of styrylbenzoxazole derivate with response to proton, *Dyes Pigm.*, 2015, **112**, 255–261.

61 K. Li, R. H. Yu, C. M. Shi, F. R. Tao, T. D. Li and Y. Z. Cui, Electrospun nanofibrous membrane based on AIE-active compound for detecting picric acid in aqueous solution, *Sens. Actuators, B*, 2018, **262**, 637–645.

62 X. C. Sun, X. Y. Ma, C. V. Kumar and Y. Lei, Protein-based sensitive, selective and rapid fluorescence detection of picric acid in aqueous media, *Anal. Methods*, 2014, **6**, 8464–8468.

63 A. S. Tanwar, S. Hussain, A. H. Malik, M. A. Afroz and P. K. Iyer, Inner filter effect based selective detection of nitroexplosive-picric acid in aqueous solution and solid support using conjugated polymer, *ACS Sens.*, 2016, **1**, 1070–1077.

64 V. Bhalla, A. Gupta, M. Kumar, D. S. S. Rao and S. K. Prasad, Self-assembled pentacenequinone derivative for trace detection of picric acid, *ACS Appl. Mater. Interfaces*, 2013, **5**, 672–679.

65 A. H. Malik, S. Hussain, A. Kalita and P. K. Iyer, Conjugated polymer nanoparticles for the amplified detection of nitro-explosive picric acid on multiple platforms, *ACS Appl. Mater. Interfaces*, 2015, **7**, 26968–26976.